

# Topological changes in glassy GeSe<sub>2</sub> at pressures up to 9.3 GPa determined by high-energy x-ray and neutron diffraction measurements

Q. Mei,<sup>1,2</sup> C. J. Benmore,<sup>1,3,\*</sup> R. T. Hart,<sup>1</sup> E. Bychkov,<sup>4</sup> P. S. Salmon,<sup>5</sup> C. D. Martin,<sup>6</sup> F. M. Michel,<sup>6</sup> S. M. Antao,<sup>6</sup> P. J. Chupas,<sup>7</sup> P. L. Lee,<sup>3</sup> S. D. Shastri,<sup>3</sup> J. B. Parise,<sup>6</sup> K. Leinenweber,<sup>2</sup> S. Amin,<sup>2</sup> and J. L. Yarger<sup>2</sup>

<sup>1</sup>*Intense Pulsed Neutron Source, Argonne National Laboratory, Argonne, Illinois 60439, USA*

<sup>2</sup>*Department of Chemistry and Biochemistry, Arizona State University, Tempe, Arizona 85287-1604, USA*

<sup>3</sup>*Advanced Photon Source, Argonne National Laboratory, Argonne, Illinois 60439, USA*

<sup>4</sup>*LPCA, UMR 8101 CNRS, Université du Littoral, 59140 Dunkerque, France*

<sup>5</sup>*Department of Physics, University of Bath, Bath BA2 7AY, United Kingdom*

<sup>6</sup>*Center for Environmental Molecular Science (CEMS), Department of Geosciences, Stony Brook University, Stony Brook, New York 11794, USA*

<sup>7</sup>*Materials Science Division, Argonne National Laboratory, Argonne, Illinois 60439, USA*

(Received 23 February 2006; revised manuscript received 8 May 2006; published 11 July 2006)

Monochromatic high-energy x-ray diffraction measurements employing microfocusing optics were performed on glassy GeSe<sub>2</sub> in a diamond anvil cell at pressures up to 9.3 GPa. In addition, the method of isotopic substitution in neutron diffraction was applied to samples that had been densified by 4% via pressurization to 10 GPa in a multianvil device and subsequently recovered to ambient conditions. The results reveal a steady increase with pressure of the average coordination number of Ge from 4.0(2) under ambient conditions to 4.5(2) at 9.3 GPa. With increasing pressure, the first sharp diffraction peak in the measured diffraction patterns at  $\sim 1.0 \text{ \AA}^{-1}$  decreases in intensity and almost disappears while the amplitude of the peaks beyond the nearest neighbor in the measured total pair distribution functions gradually increases. Equation of state measurements show a gradual density increase of 33% from ambient pressure to 8.5 GPa which is in good agreement with molecular dynamics simulations. The results are consistent with the occurrence of two densification processes for glassy GeSe<sub>2</sub>, namely, a conversion from edge-sharing to corner-sharing tetrahedra and a gradual increase in the average local coordination number with increasing density.

DOI: [10.1103/PhysRevB.74.014203](https://doi.org/10.1103/PhysRevB.74.014203)

PACS number(s): 61.43.Fs, 61.10.Nz, 61.12.Ld

## I. INTRODUCTION

GeSe<sub>2</sub> is an archetypal network glass that has long been the subject of both experimental and theoretical interest. Early diffraction experiments<sup>1,2</sup> and molecular dynamics simulations<sup>3,4</sup> led to a description of the glass structure in terms of Ge(Se<sub>4</sub>)<sub>1/2</sub> tetrahedra that share both edges and corners, to give a distribution of rings containing predominantly three, six, seven, or eight Ge atoms. However, unlike oxide glasses, the GeSe<sub>2</sub> network contains a significant number of “wrong” or homopolar bonds that enable a greater variety of local packing arrangements.<sup>5,6</sup> The local structural motifs arrange to form ordering on an intermediate scale which manifests itself by the appearance of a so-called first sharp diffraction peak (FSDP) in the measured structure factor at a scattering vector  $Q_1 \sim 1.0 \text{ \AA}^{-1}$ .<sup>7</sup> In addition to this ordering, which has a periodicity  $\sim 2\pi/Q_1$ , extended range ordering in real space has recently been found, which is associated with the principal peak at  $Q \sim 2 \text{ \AA}^{-1}$  and which extends to distances well beyond the intermediate range.<sup>8,9</sup>

On melting GeSe<sub>2</sub>, an increase in temperature is first accompanied by an increase in the density.<sup>10</sup> Neutron diffraction experiments show a breakdown of the associated intermediate range order, as signified by the disappearance of the FSDP,<sup>11,12</sup> and molecular dynamics simulations point to an accompanying increase in the number of homopolar bonds.<sup>13</sup> X-ray diffraction experiments on the liquid also show a breakdown of the intermediate-range order with increasing pressure and have led to the suggestion that GeSe<sub>2</sub> undergoes

a (first-order) liquid-liquid transition at high pressures in which there is a change from a two-dimensional (2D) network to a three-dimensional (3D) networklike fluid.<sup>14</sup> We have therefore been motivated to perform neutron and x-ray diffraction experiments to investigate the effect of pressure on the structure of glassy GeSe<sub>2</sub>. This material is more covalent than its oxide counterpart, GeO<sub>2</sub>, e.g., the ionicity of the Ge-Se and Ge-O bonds on the Pauling electronegativity scale is 7% and 40%, respectively. Glassy GeSe<sub>2</sub> might therefore be expected to exhibit quite different behavior from GeO<sub>2</sub>, which transforms from a tetrahedral to an octahedral glass with the application of pressure.<sup>15,16</sup>

Raman scattering experiments on glassy GeSe<sub>2</sub> show little change in the frequency of modes due to corner-shared Ge(Se<sub>4</sub>)<sub>1/2</sub> tetrahedral units with increasing pressure until  $\sim 3$  GPa after which the modes show a steady increase in frequency.<sup>17</sup> The measured scattering strength ratio of the modes indicates a steady increase in the ratio of corner- to edge-sharing tetrahedra with increasing pressure up until  $\sim 3$  GPa after which the ratio remains approximately constant. Raman spectroscopy data for permanently densified GeSe<sub>2</sub> glass, subjected to a pressure of 10 GPa and recovered to ambient conditions, also show a conversion from edge- to corner-sharing tetrahedra, which indicates significant changes in the distribution of ring structures within the glassy network.<sup>18</sup> *In situ* electrical resistivity measurements on glassy GeSe<sub>2</sub> by Prasad *et al.*<sup>19,20</sup> show a discontinuity at 7 GPa, which was attributed to a transition from glassy semiconductor to crystalline metal, the phases being determined

by x-ray diffraction experiments on the starting and recovered samples. By contrast, recent *ab initio* molecular dynamics simulations predict that GeSe<sub>2</sub> will remain in an amorphous state up to 75 GPa.<sup>21</sup> Between ambient pressure and 13 GPa, the simulations show that the amount of chemical disorder, as represented by Ge-Ge and Se-Se homopolar bonds, is reduced, and the topological disorder of the network increases. At higher pressures, there is gradual formation of an amorphous metallic state which is associated with a local coordination change of both the Ge and Se atoms and an increase in the number of homopolar bonds. Temperature is also known to have a large influence on structure in this system: Shimada and Datchile<sup>22</sup> have synthesized three different crystalline polymorphs by subjecting glassy GeSe<sub>2</sub> to temperatures between 300 and 600 °C and pressures up to 8 GPa over the course of 1 to 2 days.

In the present work we have used a microfocused high-energy x-ray beam, of vertical dimension  $\sim 30 \mu\text{m}$ , together with a diamond anvil cell, to perform *in situ* high-pressure x-ray diffraction experiments.<sup>23</sup> Combined with an image plate detector system, relatively high-quality structure factors can be reliably measured over a wide scattering vector range of  $\sim 0.5$  to  $17 \text{ \AA}^{-1}$  in approximately 1 h per pressure point up to a maximum pressure of 9.3 GPa. To help elucidate the mechanism behind the collapse of the tetrahedral network, neutron diffraction studies using the isotopic substitution method<sup>24</sup> have also been employed to extract detailed structural information from very small GeSe<sub>2</sub> samples that have been pressurized and recovered to ambient conditions. Our results show that GeSe<sub>2</sub> remains amorphous up to at least 9.3 GPa, in conflict with the results of Prasad *et al.*,<sup>19,20</sup> and that structural changes take place by a combination of conversion from edge- to corner-sharing Ge(Se<sub>4</sub>)<sub>1/2</sub> tetrahedral units and an increase in the local coordination number.

## II. THEORY

The quantity extracted in a neutron diffraction experiment is the total structure factor  $S_N(Q)$  which is given by

$$S_N(Q) = \frac{1}{\langle b \rangle^2} \sum_{\alpha, \beta} c_\alpha c_\beta b_\alpha b_\beta S_{\alpha\beta}(Q), \quad (1)$$

where  $c_\alpha$  and  $b_\alpha$  are the atomic fraction and coherent scattering length of chemical species  $\alpha$  and  $S_{\alpha\beta}(Q)$  denotes the so-called Faber-Ziman partial structure factor.<sup>25</sup> The total bound coherent scattering length of the sample is given by  $\langle b \rangle = \sum_\alpha c_\alpha b_\alpha$ . The analogous pseudonuclear x-ray total structure factor  $S_X(Q)$  is obtained by replacing  $b_\alpha$  by  $f_\alpha(Q)$  in Eq. (1), where  $f_\alpha(Q)$  represents the  $Q$ -dependent atomic form factor of chemical species  $\alpha$ .<sup>26,27</sup> The term ‘‘pseudonuclear’’ is used as it is assumed that the electron density of each atom is spherical and concentric with the nucleus in order to deduce the nuclear positions.

For an x-ray diffraction experiment the weighting factors of the  $S_{\alpha\beta}(Q)$  are very similar since the atomic numbers are  $Z(\text{Ge})=32$  and  $Z(\text{Se})=34$ . In the case of a neutron diffraction experiment on a sample with natural isotopic abundances of the elements,  $^{\text{nat}}\text{Ge}^{\text{nat}}\text{Se}_2$ , the weighting factors of the  $S_{\alpha\beta}(Q)$

are also very similar since the coherent neutron scattering lengths are  $b(^{\text{nat}}\text{Ge})=8.185(20)$  fm and  $b(^{\text{nat}}\text{Se})=7.970(9)$  fm.<sup>28</sup> Hence both  $S_N(Q)$  and  $S_X(Q)$  closely approximate the Bhatia-Thornton<sup>29</sup> number-number partial structure, factor  $S_{NN}^{\text{BT}}(Q)$ , which describes the topology of the system,<sup>30–32</sup> i.e.,

$$\begin{aligned} S_{\text{nat}}^{\text{nat}} S_N(Q) &= 0.115(1) S_{\text{GeGe}}(Q) + 0.437(6) S_{\text{SeSe}}(Q) \\ &+ 0.448(3) S_{\text{GeSe}}(Q), \end{aligned} \quad (2)$$

where  $S_{\text{nat}}^{\text{nat}} S_N(Q) \approx S_{NN}^{\text{BT}}(Q) \approx S_X(Q)$ . The measured neutron and x-ray total structure factors  $S_N(Q)$  and  $S_X(Q)$  are related to the corresponding total pair distribution functions  $G_N(r)$  and  $G_X(r)$  via Fourier transformation.<sup>7</sup>

More detailed structural information can be obtained by applying the method of isotopic substitution in neutron diffraction.<sup>5,6,24</sup> By measuring the diffraction patterns for samples that are identical in every respect, except that selenium of natural isotopic abundance,  $^{\text{nat}}\text{Se}$ , is replaced by selenium enriched with the  $^{76}\text{Se}$  isotope having a scattering length  $b(^{76}\text{Se})=12.2(1)$  fm, a direct subtraction of the total structure factors will eliminate the Ge-Ge correlations to give the first-order difference function

$$\begin{aligned} \Delta S_N^{\text{Se}}(Q) &\equiv \frac{\langle ^{76}_{\text{nat}} b \rangle^2 \text{}^{76} S(Q) - \langle ^{\text{nat}}_{\text{nat}} b \rangle^2 \text{}^{\text{nat}} S(Q)}{\langle ^{76}_{\text{nat}} b \rangle^2 - \langle ^{\text{nat}}_{\text{nat}} b \rangle^2} \\ &= 0.286(2) S_{\text{GeSe}}(Q) + 0.713(8) S_{\text{SeSe}}(Q), \end{aligned} \quad (3)$$

where  $\langle ^{76}_{\text{nat}} b \rangle$  and  $\langle ^{\text{nat}}_{\text{nat}} b \rangle$  denote the total bound coherent scattering lengths of the  $^{\text{nat}}\text{Ge}^{\text{nat}}\text{Se}_2$  and  $^{\text{nat}}\text{Ge}^{76}\text{Se}_2$  samples, respectively. Similarly, the Se-Se correlations can be eliminated by forming the first-order difference function

$$\begin{aligned} \Delta S_N^{\text{Ge}}(Q) &\equiv \frac{[2.344 \langle ^{\text{nat}}_{\text{nat}} b \rangle^2 \text{}^{\text{nat}} S(Q)] - \langle ^{76}_{\text{nat}} b \rangle^2 \text{}^{76} S(Q)}{(2.344 \langle ^{\text{nat}}_{\text{nat}} b \rangle^2) - \langle ^{76}_{\text{nat}} b \rangle^2} \\ &= 0.702(2) S_{\text{GeSe}}(Q) + 0.298(8) S_{\text{GeGe}}(Q). \end{aligned} \quad (4)$$

In real space, the first-order difference functions  $\Delta G_N^{\text{Se}}(r)$  and  $\Delta G_N^{\text{Ge}}(r)$  are obtained from Eqs. (3) and (4), respectively, by replacing the  $S_{\alpha\beta}(Q)$  with the corresponding partial pair distribution functions  $g_{\alpha\beta}(r)$ .

## III. EXPERIMENT

GeSe<sub>2</sub> glasses were synthesized from high-purity elements (Ge 99.9999%, Se 99.999%, Aldrich Chemicals Ltd.) at the Université du Littoral, France using established methods.<sup>33</sup> The elements were placed in thin-walled silica tubes of 8 mm inner diameter and sealed at a residual pressure below  $\approx 10^{-4}$  Torr. The silica tubes were previously cleaned using a K<sub>2</sub>CrO<sub>4</sub>-H<sub>2</sub>SO<sub>4</sub> mixture, thoroughly washed with hot distilled water, rinsed with demineralized high-purity water and dried at 150 °C. The physically adsorbed water and gases were removed under vacuum at 950 °C before using the tubes for glass synthesis. The melts were periodically stirred at 950 °C over a 48 h period. The temperature was decreased to  $\sim 800$  °C and the melts were equilibrated at that temperature for a further 24 h before quenching into water. The isotopically enriched sample

<sup>nat</sup>Ge<sup>76</sup>Se<sub>2</sub> of mass ~269 mg was made from <sup>76</sup>Se of 99.8% enrichment (Cambridge Isotopes Ltd.).

For the experiments on permanently densified samples, approximately 1 g of the <sup>nat</sup>Ge<sup>76</sup>Se<sub>2</sub> glass and 240 mg of the <sup>nat</sup>Ge<sup>76</sup>Se<sub>2</sub> glass were wrapped in vanadium foil and compressed to 10.0(4) GPa in a multianvil device at the high-pressure laboratory, Arizona State University.<sup>18</sup> The mass densities of the normal and recovered glasses were measured by immersion in toluene using the Archimedes method and were found to be 4.23(4) and 4.40(4) g cm<sup>-3</sup>, respectively, i.e., the pressurized glass was 4% denser than the as-prepared sample.

High-energy x-ray diffraction measurements were made on the as-prepared and recovered 4% densified <sup>nat</sup>Ge<sup>nat</sup>Se<sub>2</sub> and <sup>nat</sup>Ge<sup>76</sup>Se<sub>2</sub> glasses using the 11-ID-C beamline at the Advanced Photon Source (APS), Argonne National Laboratory (ANL), with an incident beam of energy 115 keV.<sup>15,34</sup> Neutron diffraction experiments were also made on the same densified glasses using the glass, liquid, and amorphous materials diffractometer (GLAD), at ANL.<sup>35</sup>

The *in situ* high-pressure x-ray diffraction measurements were conducted on beamline 1-ID at the APS, using a cryogenically cooled bent double-Laue monochromator<sup>23</sup> with an incident beam of area of 50×50 μm<sup>2</sup> and high incident beam energy of 80.0 keV. Pressure was applied to the sample using a Merrill-Bassett-type diamond anvil cell (DAC) with Be diamond anvil supports, allowing reliable diffraction patterns to be taken in a large solid angle up to a maximum scattering angle 2θ of 28° or Q~21 Å<sup>-1</sup>. The DAC was fitted with 600 μm culet anvils (type I) of length 1.2 mm and a stainless steel gasket (250 μm in thickness) was preindented to 120 μm. A sample chamber, 200 μm in diameter, was drilled into the preindented gasket by using a microelectrodischarge machining technique, creating a cavity of ~3×10<sup>-3</sup> mm<sup>3</sup>, which housed the glassy GeSe<sub>2</sub>. Two ruby crystals, each of volume about 1000 μm<sup>3</sup>, were placed in the sample container to determine the pressure using the ruby fluorescence technique,<sup>36</sup> to within an accuracy of ±10%.

The *in situ* equation of state of amorphous GeSe<sub>2</sub> was measured as a function of pressure up to 8.5 GPa using a diamond anvil cell at room temperature. A flat piece of glass with an area of approximately 5500 μm<sup>2</sup> and thickness of less than 20 μm was surrounded by a 4:1 methanol:ethanol mixture to transmit pressure under hydrostatic conditions up to 8.5 GPa. Careful consideration was used in choosing small ruby pieces and thin GeSe<sub>2</sub> samples to avoid bridging between the diamonds. Digital images of the sample loaded in the diamond cell were taken with an 8-megapixel camera (Sony DSC-F828) mounted on a microscope (Olympus BH-2) equipped with a 20× objective (Mitutoyo). By integrating the pixels in these digital images, it was possible to measure the change in area of a GeSe<sub>2</sub> sample during compression and calculate the densification by relating the change in volume to the change in area via the equation  $V/V_0 = (A/A_0)\sqrt{(A/A_0)}$  where V and V<sub>0</sub> refer to the final and initial volumes and A and A<sub>0</sub> refer to the final and initial areas, respectively.<sup>37,38</sup>

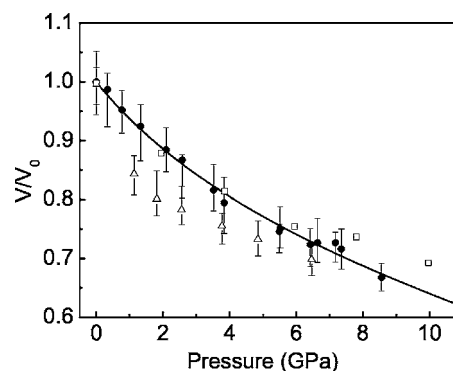


FIG. 1. Pressure-volume equation of state for amorphous GeSe<sub>2</sub>. Experimental compression in a hydrostatic medium, a 4:1 methanol:ethanol mixture (solid circles); experimental decompression from 8.55 GPa (open triangles); simulation data (open squares) (Ref. 21); third-order isothermal Birch-Murnaghan equation of state fit to the experimental compression data (solid curve).

## IV. RESULTS

### A. Glass density

The measured volume change of glassy GeSe<sub>2</sub> as a function of pressure, *P*, is shown in Fig. 1 and is compared to the volume change predicted by computer simulation.<sup>21</sup> The experimental data were fitted by using a third-order isothermal Birch-Murnaghan equation of state<sup>39</sup>

$$P = \frac{3B_0}{2} \left[ \left( \frac{V}{V_0} \right)^{-7/3} - \left( \frac{V}{V_0} \right)^{-5/3} \right] \times \left\{ 1 + \frac{3}{4}(B_1 - 4) \left[ \left( \frac{V}{V_0} \right)^{-2/3} - 1 \right] \right\}, \quad (5)$$

where the isothermal bulk modulus  $B_0 = 14.22(1.81)$  GPa and the first pressure derivative  $B_1 = 2.63(0.51)$  at 298 K.

### B. High-energy x-ray diffraction experiments on densified GeSe<sub>2</sub> glass

The 4% densified <sup>nat</sup>Ge<sup>nat</sup>Se<sub>2</sub> and <sup>nat</sup>Ge<sup>76</sup>Se<sub>2</sub> samples were investigated using high-energy x-ray diffraction with a point Ge detector. Corrections were made for the geometry, detector dead time, and polarization, and the measured photon intensity was normalized to the sum of the atomic form factors and Compton scattering as described elsewhere.<sup>40</sup> As shown in Fig. 2, there was a negligible difference between the  $S_x(Q)$  functions measured for the 4% densified <sup>nat</sup>Ge<sup>nat</sup>Se<sub>2</sub> and <sup>nat</sup>Ge<sup>76</sup>Se<sub>2</sub> glasses. However, by comparison with the normal density glass, the FSDP shifts from  $Q_1 = 0.99(1)$  to  $1.04(2)$  Å<sup>-1</sup> and undergoes a 36% reduction in peak height as measured after subtracting a linear baseline. Beyond the FSDP, the other features are quite similar except that the peak positions up to 10 Å<sup>-1</sup> shift to higher *Q* by ~0.05 Å<sup>-1</sup> without change of intensity. Since the FSDP in the normal density glass arises mainly from Ge-Ge correlations,<sup>5,6</sup> pressure appears to result in changes in the packing of the tetrahedral units and associated ring statistics.

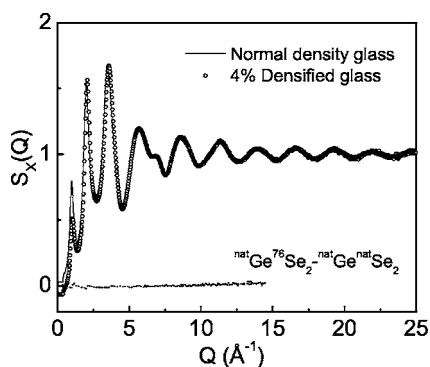


FIG. 2. Comparison between the structure factors measured using high-energy x rays,  $S_X(Q)$ , for normal density  $\text{GeSe}_2$  glass (taken from Ref. 18) and 4% densified  $\text{GeSe}_2$  glass. Also shown is the difference between the  $S_X(Q)$  functions measured for the 4% densified  ${}^{\text{nat}}\text{Ge}^{76}\text{Se}_2$  and  ${}^{\text{nat}}\text{Ge}^{\text{nat}}\text{Se}_2$  glassy samples.

### C. Neutron diffraction experiments on densified $\text{GeSe}_2$ glass

A relatively small volume of 4% densified  ${}^{\text{nat}}\text{Ge}^{76}\text{Se}_2$  sample was used for the neutron diffraction measurements ( $\sim 60 \text{ mm}^3$  compared to typical neutron diffraction samples of a few  $\text{cm}^3$  in size) together with a larger volume of 4% densified  ${}^{\text{nat}}\text{Ge}^{\text{nat}}\text{Se}_2$  sample ( $\sim 250 \text{ mm}^3$  made by combining four separately compressed samples). Corrections were made using standard analysis methods<sup>41</sup> for the container scattering, attenuation and multiple and inelastic scattering. Careful attention was paid to the background and attenuation corrections, especially for the  ${}^{\text{nat}}\text{Ge}^{76}\text{Se}_2$  sample which has a large absorption cross section associated with  ${}^{76}\text{Se}$ ,  $\sigma_{\text{abs}}({}^{76}\text{Se})=85(7)$  barn at an incident neutron wavelength of  $1.798 \text{ \AA}$ .<sup>28</sup> In the analysis of the data, both the number density and sample volume were systematically adjusted to ensure that the background and vanadium can scattering were properly subtracted such that the diffraction patterns measured for the different detector groups, which cover different angular ranges, overlap at all  $Q$  values including the low- $Q$  region. However, by comparing each measured total neutron structure factor  $S_N(Q)$  with the Fourier backtransform of the corresponding  $G_N(r)$  once the unphysical low- $r$  oscillations below  $r_{\text{min}}=2.0 \text{ \AA}$  are set to zero, significant slopes are observed [see Fig. 3(a)]. These slopes may result from geometrical effects<sup>42</sup> that arise from normalizing the scattering from the small cubic-shaped samples to the scattering from a cylindrical vanadium rod and, in the case of the  ${}^{\text{nat}}\text{Ge}^{76}\text{Se}_2$  sample, from a lack of knowledge of the wavelength dependence of the cross section of  ${}^{76}\text{Se}$ .<sup>43</sup>

The first-order difference function with the Ge-Ge partial structure factor removed,  $\Delta S_N^{\text{Se}}(Q)$ , is shown in Fig. 3(b) for the normal density and 4% densified glasses. The main effect of pressure results in a significant reduction in height of the peaks at  $Q=2.04(7)$  and  $3.52(2) \text{ \AA}^{-1}$ . However, as shown by the comparison of Fig. 2, changes at these  $Q$  values are not observed between the  $S_X(Q)$  functions measured for the normal density and densified samples. We therefore conclude that the observed decreases in the Se-related partial structure factors at  $Q \sim 2$  and  $3.5 \text{ \AA}^{-1}$  upon densification are offset by

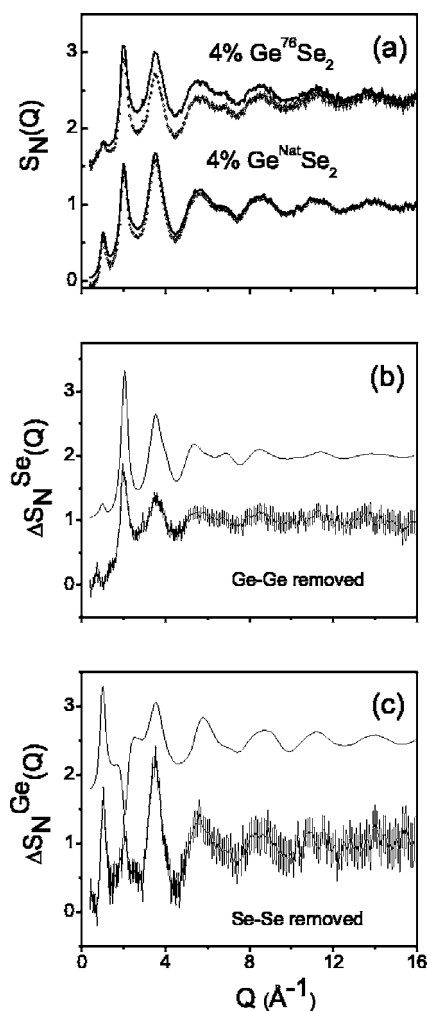


FIG. 3. (a) The total structure factors measured using neutron diffraction for 4% densified  ${}^{\text{nat}}\text{Ge}^{76}\text{Se}_2$  glass (upper data sets) and 4% densified  ${}^{\text{nat}}\text{Ge}^{\text{nat}}\text{Se}_2$  glass (lower data sets). The open circles with error bars give the measured data points and the solid curves give the Fourier backtransforms of the corresponding total pair distribution function  $G_N(r)$  after the low- $r$  oscillations below  $2 \text{ \AA}$  are set to the  $G_N(r=0)$  limit. The first-order difference function with (b) the Ge-Ge partial structure factor and (c) the Se-Se partial structure factor removed. The upper solid curves show the results for glassy  $\text{GeSe}_2$  at normal density (Refs. 5 and 6) and the lower curves with error bars show the results for 4% densified glassy  $\text{GeSe}_2$ . In (b) and (c) the difference functions for the densified glass were obtained from the solid curves in (a) and, for clarity of presentation, the functions are shown with a binning of  $\Delta Q=0.025 \text{ \AA}^{-1}$  for  $Q \leq 5 \text{ \AA}^{-1}$  and  $\Delta Q=0.05 \text{ \AA}^{-1}$  for  $Q > 5 \text{ \AA}^{-1}$ .

a change in the Ge-related partial structure factors. This is supported by the first-order difference function  $\Delta S_N^{\text{Ge}}(Q)$  with the Se-Se partial structure factor removed [see Fig. 3(c)]. The dip at  $Q=2.04(7) \text{ \AA}^{-1}$  in  $\Delta S_N^{\text{Ge}}(Q)$  for the normal density glass becomes a peak for the densified glass and there is a strong increase in the intensity of the peak at  $Q=3.5 \text{ \AA}^{-1}$  for the compressed glass.

The corresponding pair distribution functions  $\Delta G_N^{\text{Se}}(r)$  and  $\Delta G_N^{\text{Ge}}(r)$  are shown in Fig. 4. The first peak in  $\Delta G_N^{\text{Se}}(r)$  (Ge-Ge correlations removed) at  $r_1=2.34(1) \text{ \AA}$  for the nor-

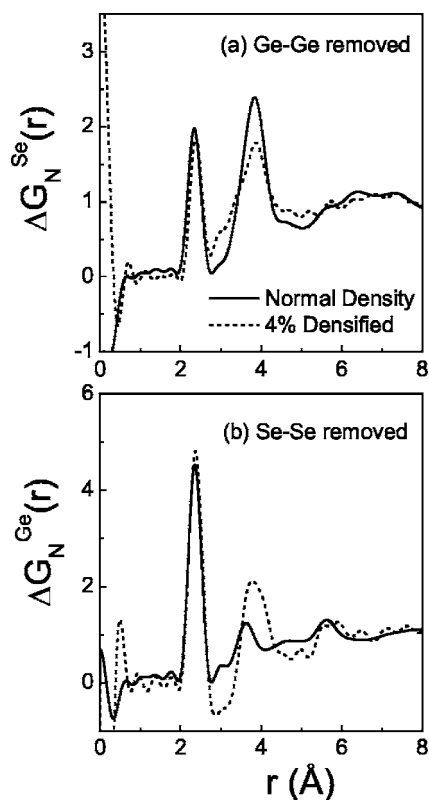


FIG. 4. Comparison between the first-order difference pair distribution functions for normal density GeSe<sub>2</sub> glass taken from Refs. 5 and 6 (solid curves) and for 4% densified GeSe<sub>2</sub> glass (broken curves). Both structure factors were truncated at  $Q_{\max}=15.9 \text{ \AA}^{-1}$  and Fourier-transformed into real space after the application of a Lorch modification function  $M(Q)=\sin(\pi Q/Q_{\max})/(\pi Q/Q_{\max})$ , which reduces Fourier-transform artifacts.

mal density glass can be attributed primarily to Ge-Se bonds (centered at 2.36 Å) but also has a contribution from Se-Se bonds at 2.32 Å.<sup>5,6</sup> This first peak shifts to a higher value of 2.37(1) Å on densification. Similarly, the first peak in  $\Delta G_N^{\text{Ge}}(r)$  (Se-Se correlations removed) at  $r_1=2.35(1) \text{ \AA}$  for the normal density glass can also be attributed primarily to Ge-Se bonds together with some homopolar Ge-Ge bonds at 2.42 Å. This peak also shifts to a higher value of 2.37(1) Å in the 4% densified glass. Both observations are consistent with a pressure-induced elongation of the main Ge-Se bond length, a pressure-dependent effect that is also found for the Ge-O bond in glassy GeO<sub>2</sub>.<sup>15</sup>

In the case of  $\Delta G_N^{\text{Se}}(r)$ , the dominant contribution to the second peak at 3.85 Å for the normal density glass arises from Se-Se correlations<sup>5,6</sup> and the broadening of this peak for the densified glass is consistent with a pressure-induced distortion of the Ge(Se<sub>4</sub>)<sub>1/2</sub> tetrahedra. The measured partial pair distribution functions for the normal density glass show a small peak at  $r \sim 3.0 \text{ \AA}$  which is attributed to the Ge-Ge distance between edge-sharing tetrahedra as well as to the possible presence of Ge-Se defects.<sup>5,6</sup> These features are not, however, discernible in the measured difference functions for the densified glass. In the case of  $\Delta G_N^{\text{Ge}}(r)$ , the second peak that is dominated by Ge-Ge correlations between corner-sharing tetrahedral centers<sup>5,6</sup> shifts from

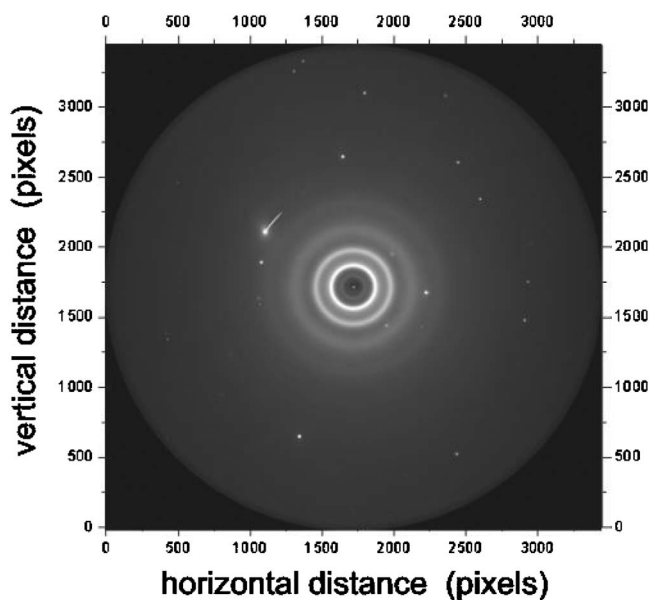


FIG. 5. Two-dimensional contour plot obtained from the Mar345 image plate detector. The data are for glassy GeSe<sub>2</sub> in a DAC at 5.3 GPa measured using incident x rays of energy 80.047 keV. The bright spots are Bragg peaks from the single-crystal diamonds and rubies while the diffuse rings show the diffraction pattern for the GeSe<sub>2</sub> glass.

3.63(1) to 3.77(2) Å in the densified glass, indicating an increase in the average Ge-Se-Ge angle between Ge(Se<sub>4</sub>)<sub>1/2</sub> tetrahedra from 98.3° (See Refs. 5 and 6) to approximately 105°.

#### D. *In situ* high-pressure high-energy x-ray diffraction experiments on GeSe<sub>2</sub> glass

Drilled diamonds were used to minimize the amount of anvil material in the beam and thereby the Compton scattering from the DAC. However, the DAC contributed many single-crystal diamond peaks to the diffraction patterns, as can be seen in the two-dimensional image from the Mar345 image-plate detector in Fig. 5, which also shows the single-crystal ruby Bragg scattering from the pressure sensors. The Bragg peaks, and the regions around them, were carefully deleted from the image plate detector before the data were reduced to intensity versus scattering angle using the program FIT2D.<sup>44</sup> The image plate was exposed for 35, 5 s intervals to avoid saturation due to the Bragg peaks (the detector readout took  $\sim 90$  s between exposures). These runs were averaged to improve the counting statistics. The integrated data were processed to obtain reliable  $S_X(Q)$  up to  $Q \sim 17 \text{ \AA}^{-1}$  by using the program<sup>45</sup> PDFGETX in which standard corrections were applied as well as those required for the image plate geometry. The large number of pixels per solid angle on the Mar345 image plate yield a small  $Q$ -space bin width of  $\Delta Q \sim 0.005 \text{ \AA}^{-1}$  compared to  $\sim 0.025 \text{ \AA}^{-1}$  for the single-Ge-detector measurements. The background correction for the *in situ* high-pressure experiments was performed by subtracting the intensity collected for the empty DAC at zero applied pressure.<sup>23</sup> Unlike our previous studies with a

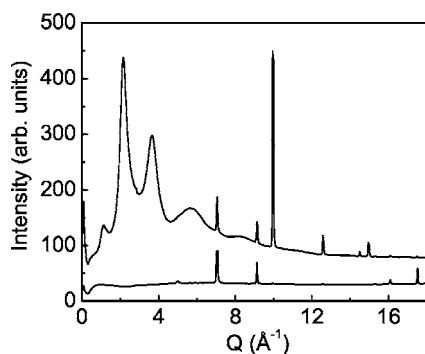


FIG. 6. The raw intensity measured using high-energy x rays for glassy  $\text{GeSe}_2$  in a diamond anvil cell at 5.3 GPa (upper curve) and for the empty diamond anvil cell at ambient pressure (lower curve). The additional sharp peaks arise from single-crystal ruby and diamond Bragg scattering, which can change in intensity as the cell is rotated slightly. These are the bright spots in Fig. 5, which are individually masked out in the analysis.

panoramic pressure cell,<sup>16</sup> the background showed only minimal changes with pressure and, therefore, no additional correction was needed. Figure 6 compares the measured x-ray intensities for the glass and diamond plus ruby sensors in the DAC at high pressure and the empty DAC at ambient pressure. The additional peaks in the range of 9–16  $\text{\AA}^{-1}$  that are absent for empty DAC diffraction pattern arise from the single-crystal ruby Bragg scattering.

The x-ray total structure factors  $S_X(Q)$  for glassy  $\text{GeSe}_2$  at pressures up to 9.3 GPa are shown in Fig. 7. The most dramatic changes with increasing pressure correspond to a decrease in intensity of the FSDP and an increase in intensity of the principal peak at  $Q \sim 2.0 \text{\AA}^{-1}$ . Between ambient pressure and 9.3 GPa, the FSDP position shifts from 1.010(5)

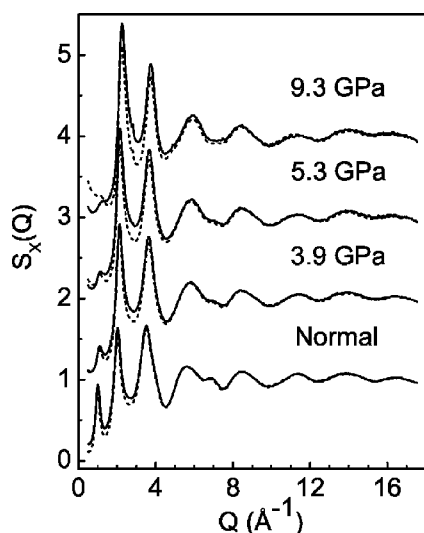


FIG. 7. The total structure factors for glassy  $\text{GeSe}_2$  at different pressures measured using *in situ* high-energy x-ray diffraction. The solid curves show the measured data and the dashed curves show the Fourier backtransforms of the corresponding total pair distribution function  $G_X(r)$  after the low- $r$  oscillations below 2  $\text{\AA}$  are set to the  $G_X(r=0)$  limit. The small Bragg peaks in the high-pressure data sets are due to residual scattering from the diamond anvils.

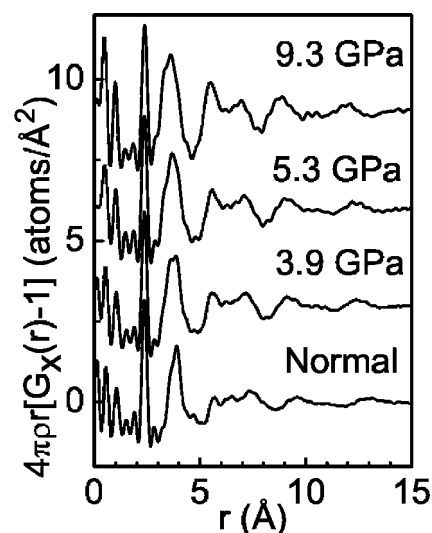


FIG. 8. The total pair distribution functions for glassy  $\text{GeSe}_2$  at different pressures as measured by *in situ* high-energy x-ray diffraction. The curves were obtained by Fourier-transforming the total structure factors of Fig. 7 after the data sets were truncated at  $Q_{\text{max}}=17 \text{\AA}^{-1}$  (no window modification function was applied).

to 1.225(5)  $\text{\AA}^{-1}$ , the second peak position shifts from 2.042(5)  $\text{\AA}^{-1}$  to higher  $Q$  by 0.22  $\text{\AA}^{-1}$ , and the intensity of this peak increases by a factor of 1.46. The higher- $Q$ -value peaks, including most notably the double peak between 4.5 and 7.5  $\text{\AA}^{-1}$ , are consistent with the appearance of well-defined tetrahedral units.<sup>46,47</sup> The weakening and gradual disappearance of the high- $Q$  shoulder at 6.92  $\text{\AA}^{-1}$  between ambient pressure and 9.3 GPa may therefore be related to a reduction in the number of regular tetrahedral units. We note that in glassy  $\text{GeO}_2$  under pressure, the double peak in the range 5–10  $\text{\AA}^{-1}$  of the x-ray structure factor coalesces into a single broad peak, once the pressure is above 6 GPa, and there is a conversion from tetrahedral to five- and sixfold-coordinated units.<sup>16</sup>

To highlight the changes that take place in the short- and intermediate-range order of glassy  $\text{GeSe}_2$  with increasing pressure, the pair distribution functions  $D_X(r)=4\pi\rho r[G_X(r)-1]$ , obtained by Fourier-transforming the  $S_X(Q)$  functions of Fig. 7, are shown in Fig. 8. The first peak at 2.364(5)  $\text{\AA}$  at ambient pressure, which has a predominant contribution from Ge-Se correlations,<sup>5,6</sup> shifts slightly to 2.376(5)  $\text{\AA}$  as the pressure is increased to 9.3 GPa (see Table I). By comparison, in liquid  $\text{GeSe}_2$  the Ge-Se nearest-neighbor peak shifts from 2.32 to 2.46  $\text{\AA}$  when the pressure is increased from ambient to 5.1 GPa.<sup>14</sup> The average Ge coordination number, calculated assuming Ge-Se correlations alone, increases from 4.0(2) to 4.2(2) between ambient pressure and 3.9 GPa, and increases further to 4.5(2) at 9.3 GPa (see Table I). Since  $G_X(r)$  approximates the Bhatia-Thornton number-number partial pair-distribution function  $g_{\text{NN}}(r)$ , the average coordination number irrespective of species type  $\bar{n}$  can also be readily deduced from<sup>12,31,32</sup>

TABLE I. Peak positions and coordination numbers for GeSe<sub>2</sub> as a function of pressure.

Pressure (GPa)	First peak position $Q_1$ ( $\text{\AA}^{-1}$ )	Second peak position $Q_2$ ( $\text{\AA}^{-1}$ )	Number density $\rho$ (atoms $\text{\AA}^{-3}$ )	First peak position in $D(r)$ ( $\text{\AA}$ )	Ratio $r_{\text{SeSe}}/r_{\text{GeSe}}$	Average Ge coordination number <sup>a</sup>	Mean coordination number $\bar{n}$
0	1.010(5)	2.042(5)	0.0334(2)	2.364(5)	1.650(5)	3.98(20)	2.59(20)
10 (recovered to 0)	1.04(2)	2.06(2)	0.0347(2)	2.347(2)	1.621(2)	4.01(20)	2.61(20)
3.9 <i>in situ</i>	1.102(5)	2.131(5)	0.0422(2)	2.360(5)	1.636(5)	4.15(20)	2.76(20)
5.3 <i>in situ</i>	1.131(5)	2.151(5)	0.0444(2)	2.362(5)	1.559(5)	4.30(20)	2.90(20)
9.3 <i>in situ</i>	1.225(5)	2.262(5)	0.0509(2)	2.376(5)	1.524(5)	4.52(20)	3.16(20)
2D crystal	1.06 <sup>b</sup>		0.0344	2.346		4.00	
3D crystal	1.27 <sup>b</sup>		0.0377	2.359		4.00	

<sup>a</sup>Assuming only Ge-Se correlations under the first peak.

<sup>b</sup>Taking the first principal peak in the Ge-Ge partial structure factor.

$$4\pi\rho \int_{r_1}^{r_2} r^2 G_X(r) dr \approx \bar{n} = c_{\text{Ge}}(\bar{n}_{\text{Ge}}^{\text{Ge}} + \bar{n}_{\text{Ge}}^{\text{Se}}) + c_{\text{Se}}(\bar{n}_{\text{Se}}^{\text{Se}} + \bar{n}_{\text{Se}}^{\text{Ge}}), \quad (6)$$

where  $\rho$  is the atomic number density and  $\bar{n}_{\alpha}^{\beta}$  is the mean coordination number of chemical species  $\beta$  around  $\alpha$  in a volume defined by two concentric spheres of radii  $r_1$  and  $r_2$ . The results also show an increase in the coordination number  $\bar{n}$  from 2.6(2) at ambient pressure to 2.8(2) at 3.9 GPa and a further increase to 3.2(2) as the pressure is raised further to 9.3 GPa (see Table I). Hence the observed increase in coordination number is independent of the assignment of the first peak in  $G_X(r)$  to specific pair correlations. We note that to calculate the coordination numbers we used a number density for the glass at 9.3 GPa which was obtained from an extrapolation using a Birch-Murnaghan equation of state fit to the compression data up to 8.5 GPa (see Fig. 1).

At ambient pressure, the second peak in  $D_X(r)$  at 3.90(1)  $\text{\AA}$  has a large contribution from Se-Se correlations at 3.90  $\text{\AA}$  which overlap with a smaller contribution from Ge-Ge correlations at 3.57  $\text{\AA}$  that arise predominantly from the centers of corner-sharing tetrahedra.<sup>5,6</sup> With the application of pressures up to 9.3 GPa the second peak broadens and shifts markedly to 3.62(2)  $\text{\AA}$ . If Ge-Se and Se-Se distances  $r_{\text{GeSe}}$  and  $r_{\text{SeSe}}$  are identified with the first and second peaks in  $D_X(r)$ , respectively, the distance ratio  $r_{\text{SeSe}}/r_{\text{GeSe}}$ , which is  $\sqrt{8/3}=1.633$  for perfect tetrahedra, changes from 1.650 at ambient pressure (the measured<sup>5,6</sup> partial pair distribution functions give a ratio of 1.647) to 1.524 at 9.3 GPa. The results are therefore consistent with a substantial distortion and breakdown of the tetrahedra during compression. The peak in  $D_X(r)$  at 5.67(3)  $\text{\AA}$  gradually shifts to 5.50(2)  $\text{\AA}$  and increases in intensity with increasing pressure, while the peak at 7.35(4)  $\text{\AA}$  moves inward to 6.95(4)  $\text{\AA}$  at the highest pressure with little change in intensity. The peaks at larger distances increase in intensity as the pressure increases and the peaks at 9.6 and  $\sim 13.0$   $\text{\AA}$  move inward to 8.8 and  $\sim 12$   $\text{\AA}$ , respectively. Overall it can be seen from Fig. 8 that the intermediate-range order in glassy GeSe<sub>2</sub> becomes more pronounced as the peaks sharpen with increasing pressure up to 9.3 GPa, although the FSDP is significantly reduced (see

Fig. 7). It is therefore plausible that this observation is associated with the growth in intensity of the principal peak at  $Q=2$   $\text{\AA}^{-1}$  in  $S_X(Q)$ .<sup>8</sup>

## V. DISCUSSION

The results of this study have revealed several aspects of network collapse in glassy GeSe<sub>2</sub> under pressure. First, GeSe<sub>2</sub> remains glassy up to at least 9.3(0.9) GPa and the pressure-volume equation of state is reasonably well described by the previous simulation data of Durandurdu and Drabold<sup>21</sup> at least up to pressures of  $\sim 6$  GPa (see Fig. 1). At larger pressures, the larger discrepancies between the experimental and computer simulation results may arise from limitations associated with use of the Parrinello-Rahman method in the molecular dynamics calculations.<sup>48</sup> Second, the *in situ* high-energy x-ray diffraction results show a large decrease in the first sharp diffraction peak with increasing pressure and a large growth of the principal peak. Changes in the real-space distribution functions indicate a distortion of the tetrahedral units and gradual formation of higher coordinate polyhedra at higher pressures. Third, the isotopic neutron and high-energy x-ray diffraction data on the recovered samples (densified at 10 GPa) show that on decompression the Ge-Se bond length remains elongated and, although the compacted samples revert back to fourfold coordination, the tetrahedra are distorted.

### A. Relation to Raman spectroscopy results

The *in situ* Raman spectroscopy results of Wang *et al.*<sup>17</sup> show that the ratio of edge- to corner-sharing tetrahedra reduces from 34% at ambient pressure<sup>5,6</sup> to  $\sim 20\%$  at  $\sim 3$  GPa, and then remains essentially the same beyond 3 GPa. The closer-packed arrangement of the GeSe<sub>2</sub> network in the pressure range 0–3 GPa is therefore associated with a conversion from edge-sharing to corner-sharing tetrahedra. Raman spectroscopy results on GeSe<sub>2</sub> samples decompressed from high pressure to ambient conditions support this change in the connectivity of the tetrahedral units.<sup>18</sup>

### B. Comparison with crystal structures

It is of interest to compare the structural changes under pressure in GeSe<sub>2</sub> glass with those found in the crystalline

material. At ambient pressure,  $\beta$ -GeSe<sub>2</sub> consists of layers that comprise chains of corner-sharing Ge(Se<sub>4</sub>)<sub>1/2</sub> tetrahedra along the  $a$  axis that are linked by edge-sharing tetrahedra along the  $b$  axis.<sup>49,50</sup> Upon compression to 9 GPa at 573–1173 K, two phase transitions in crystalline  $\beta$ -GeSe<sub>2</sub> have been observed.<sup>50</sup> The first transition occurs at  $\sim 3$  GPa and is associated with a transformation to a cristobalitelike structure which comprises only corner-sharing tetrahedra, i.e., there is a change from a 2D to a 3D type of structure. The x-ray diffraction patterns of  $\beta$ -GeSe<sub>2</sub> and cristobalitelike GeSe<sub>2</sub> show a shift in the first Bragg peak position from 1.06 to 1.27 Å<sup>-1</sup> with a decrease in intensity,<sup>51</sup> similar to the shifts observed for the FSDP in glassy GeSe<sub>2</sub> in the present work (see Table I). The second transformation of crystalline GeSe<sub>2</sub>, which occurs in the range 5–7 GPa, is associated with a change in the coordination number of the Ge atoms from 4 to 6 and the resultant crystal has a distorted layered structure analogous to CdI<sub>2</sub>. However, this high-pressure phase is unstable and the full crystal structure has not yet been determined.<sup>52</sup> We note that the Ge-Se distance in the Ge(Se<sub>1/2</sub>)<sub>4</sub> tetrahedra of  $\beta$ -GeSe<sub>2</sub> is 2.36 Å,<sup>49</sup> and the Ge-Se distance in the six-coordinated GeSe<sub>2</sub> system is 2.87 Å.<sup>14</sup> Pressure-induced phase transitions in crystalline GeSe<sub>2</sub>, including the semiconductor-to-metal transition at high pressure, have been investigated by *ab initio* methods.<sup>48,53</sup>

The isothermal bulk modulus  $B_0=14.22(1.81)$  GPa and first pressure derivative  $B_1=2.63(0.51)$  measured for the glassy phase of GeSe<sub>2</sub> at 298 K compare with values of 11.5(2.2) GPa and 9.1(2.2) obtained from a third-order Birch-Murnaghan fit to the x-ray diffraction data of Stølen *et al.*<sup>54</sup> for the  $\beta$ -GeSe<sub>2</sub> crystalline phase at 573 K. The large  $B_1$  value for the crystalline phase is expected from its anisotropic layered structure and, if it is restricted to 4.0, a larger value of  $B_0=17.6(0.7)$  GPa is instead obtained from the Birch-Murnaghan fit.<sup>54</sup> The density under ambient conditions of the glass, 4.23(4) g cm<sup>-3</sup>, is smaller than that of the  $\beta$ -GeSe<sub>2</sub> crystalline phase either at room temperature, 4.37 g cm<sup>-3</sup>,<sup>49</sup> or at 573 K, 4.33 g cm<sup>-3</sup>.<sup>54</sup> A smaller compressibility and larger bulk modulus for the crystalline phase is therefore anticipated.

### C. Comparison with the structure of germanium dioxide

The structure of glassy GeO<sub>2</sub> under pressure shows several qualitative similarities to glassy GeSe<sub>2</sub>. For example, neutron diffraction experiments show that with increasing pressure the intensity of the FSDP decreases, the FSDP peak position moves to larger  $Q$  values, and the nearest-neighbor bond distance increases.<sup>16</sup> However the mechanisms for densification are quite different in each case. In GeO<sub>2</sub> below 6 GPa, the cage structures formed by corner-sharing tetrahedra collapse with increasing pressure, enabled by a rotation of the tetrahedra around the Ge-O-Ge bond.<sup>15</sup> This is followed by a gradual coordination number change around Ge from 4 to 6 over the pressure range 6–15 GPa, via a mixture of four-, five-, and sixfold-coordinated species.<sup>16</sup> By comparison, in GeSe<sub>2</sub> glass there are edge-sharing tetrahedra that convert to corner-sharing tetrahedra up to 3 GPa and, from ambient pressure to 9.3 GPa, there is a steady increase in the

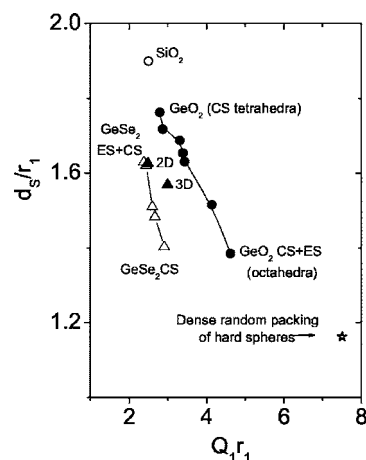


FIG. 9. The relationship between the first sharp diffraction peak position  $Q_1$  and the mean atomic spacing  $d_S$  deduced from  $d_S^3 = (6/\pi\rho)$  where  $\rho$  is the atomic number density. Both functions are scaled by the nearest-neighbor bond distance  $r_1$ , as obtained from the first peak position in the measured pair distribution functions. The results are compared for glassy GeSe<sub>2</sub> (open triangles), crystalline GeSe<sub>2</sub> (solid triangles, see Table I), and glassy GeO<sub>2</sub> at ambient pressure and for a dense random packing of hard spheres Ref. 47. CS and ES refer to corner- and edge-sharing polyhedra, respectively.

coordination number of Ge from 4.0(2) to 4.5(2). The differences in the pressure-dependent properties of GeSe<sub>2</sub> and GeO<sub>2</sub> can be attributed to the higher ionicity of the oxide glass, where corner sharing is the only method of connecting the tetrahedral units and the only way to pack the network more efficiently, once the void space is taken up, is to increase the coordination number. The ability of GeSe<sub>2</sub> to form homopolar Ge-Ge and Se-Se bonds and convert from edge- to corner-shared tetrahedral motifs provides additional mechanisms by which densification may occur.

It has been suggested by Benmore *et al.*<sup>47</sup> that a plot of  $d_S/r_1$  vs  $Q_1r_1$ , where  $d_S$  is the mean atomic spacing  $d_S^3 = (6/\pi\rho)$  and  $\rho$  is the atomic number density, can be used to observe similarities between the intermediate-range order in different types of glasses and liquids with increasing density. In Fig. 9 we show this plot in order to compare the data for GeSe<sub>2</sub> and GeO<sub>2</sub> as a function of pressure (density). For several systems that form tetrahedral networks, the trend with increasing density is for the scaled FSDP position to approach that expected for a dense random packing of hard spheres.<sup>47</sup> However, the curve for GeSe<sub>2</sub> does not display this behavior but instead runs roughly parallel to the curve for GeO<sub>2</sub>. Also, for the liquid phase of GeSe<sub>2</sub>, a change in the connectivity of the liquid from 2D to 3D with increasing pressure has been reported.<sup>14</sup> However, the curve for the glassy phase of GeSe<sub>2</sub> does not follow the curve for the crystalline phase for which there is a transition from a 2D to 3D arrangement of Ge(Se<sub>4</sub>)<sub>1/2</sub> tetrahedra with increasing density. Further studies of GeSe<sub>2</sub> are needed at higher pressures to see if higher-density amorphous forms are achievable (closer to the dense random packing limit) or whether the glass immediately crystallizes. It would also be informa-

tive to understand the changes in ring statistics during the conversion from edge- to corner-sharing tetrahedra with increasing density as this conversion presumably acts as a way of introducing greater flexibility into the network, allowing the ring structures to change and fill space. However, does densification result from the rings becoming larger with increasing pressure as suggested by Hobbs *et al.* for glassy SiO<sub>2</sub>,<sup>55</sup> or does it result from an increase in the number of smaller rings, as proposed by Wright *et al.*<sup>56</sup> for the case of radiation-densified silica glass? Furthermore, what is the role played by homopolar bonds? For example, the molecular dynamics simulations of Durandurdu and Drabold<sup>21</sup> show that homopolar bonds are present and that there is a significant increase in their number at pressures above 12 GPa.

## VI. CONCLUSIONS

The measured density of glassy GeSe<sub>2</sub> increases smoothly by 33% between ambient pressure and 8.5 GPa and the data compare reasonably well with the *ab initio* molecular dynamics simulations of Durandurdu and Drabold.<sup>21</sup> *In situ* high-pressure x-ray diffraction studies show that GeSe<sub>2</sub> is still amorphous at 9.3 GPa, contrary to the earlier conclusions of Prasad *et al.*<sup>19,20</sup> which were based on an x-ray diffraction analysis of recovered samples. The first sharp diffraction peak in the measured total structure factor shows a significant decrease in height to ~31% of its original value as the pressure is increased from ambient to 3.9 GPa, but shows a much smaller change of 8% between 3.9 and 9.3 GPa. These changes are accompanied by a significant increase in intensity of the principal peak at ~2 Å<sup>-1</sup> and an increase in amplitude of the peaks beyond the nearest neigh-

bor in the total pair distribution functions. The average coordination number of Ge increases approximately linearly from 4.0(2) at ambient pressure to 4.5(2) at 9.3 GPa and Raman spectroscopy results show a pressure-induced conversion from edge- to corner-sharing Ge(Se<sub>4</sub>)<sub>1/2</sub> tetrahedra.<sup>17,18</sup> The diffraction results show that this conversion is accompanied by an elongation of the mean Ge-Se bond length and a substantial distortion of the Ge(Se<sub>4</sub>)<sub>1/2</sub> tetrahedra.

The diffraction and Raman spectroscopy results for glassy GeSe<sub>2</sub> are therefore consistent with the occurrence of two densification processes, namely, (i) a conversion from edge- to corner-sharing tetrahedra and (ii) a gradual increase in the average local coordination number with increasing density. Moreover, we observe in the total pair correlation functions an increase in the intermediate-range order with increasing pressure (up to 9.3 GPa) which is accompanied by a decrease in intensity of the FSDP. Finally, the quality of the high-pressure DAC diffraction data obtained by using microfocused high-energy x-ray beams shows that this method provides a means of probing the structure of glasses and liquids at extreme pressures.

## ACKNOWLEDGMENTS

This work is supported by the U.S. DOE, NSF (Grant No. EAR-0510501 and No. DMR-0452444), DOD, and the Keck Foundation, through measurements performed at the IPNS and APS Divisions, Argonne National Laboratory, under Contract No. W31109-ENG 38. Ning Yang is gratefully thanked for helpful discussion during the high-energy x-ray data analysis.

\*Corresponding author. FAX: 630 252 4163. Electronic address: benmore@anl.gov

<sup>1</sup>S. Susman, D. L. Price, K. J. Volin, R. J. Dejus, and D. G. Montague, *J. Non-Cryst. Solids* **106**, 26 (1988).

<sup>2</sup>S. Susman, K. J. Volin, D. G. Montague, and D. L. Price, *J. Non-Cryst. Solids* **125**, 168 (1990).

<sup>3</sup>P. Vashishta, R. K. Kalia, G. A. Antonio, and I. Ebbsjö, *Phys. Rev. Lett.* **62**, 1651 (1989).

<sup>4</sup>P. Vashishta, R. K. Kalia, and I. Ebbsjö, *Phys. Rev. B* **39**, 6034 (1989).

<sup>5</sup>I. Petri, P. S. Salmon, and H. E. Fischer, *Phys. Rev. Lett.* **84**, 2413 (2000).

<sup>6</sup>P. S. Salmon and I. Petri, *J. Phys.: Condens. Matter* **15**, S1509 (2003).

<sup>7</sup>P. S. Salmon, *Proc. R. Soc. London, Ser. A* **445**, 351 (1994).

<sup>8</sup>P. S. Salmon, R. A. Martin, P. E. Mason, and G. J. Cuello, *Nature (London)* **435**, 75 (2005).

<sup>9</sup>P. S. Salmon, *J. Phys.: Condens. Matter* **17**, S3537 (2005).

<sup>10</sup>J. Ruska and H. Thurn, *J. Non-Cryst. Solids* **22**, 277 (1976).

<sup>11</sup>I. T. Penfold and P. S. Salmon, *Phys. Rev. Lett.* **67**, 97 (1991).

<sup>12</sup>I. Petri, P. S. Salmon, and W. S. Howells, *J. Phys.: Condens. Matter* **11**, 10219 (1999).

<sup>13</sup>C. Massobrio, F. H. M van Roon, A. Pasquarello, and S. W. De

Leeuw, *J. Phys.: Condens. Matter* **12**, L697 (2000).

<sup>14</sup>W. A. Crichton, M. Mezouar, T. Grande, S. Stølen, and A. Grzechnik, *Nature (London)* **414**, 622 (2001).

<sup>15</sup>S. Sampath, C. J. Benmore, K. M. Lantzky, J. Neufeind, K. Leinenweber, D. L. Price, and J. L. Yarger, *Phys. Rev. Lett.* **90**, 115502 (2003).

<sup>16</sup>M. Guthrie, C. A. Tulk, C. J. Benmore, J. Xu, J. L. Yarger, D. D. Klug, J. S. Tse, H.-k. Mao, and R. J. Hemley, *Phys. Rev. Lett.* **93**, 115502 (2004).

<sup>17</sup>F. Wang, S. Mamedov, P. Boolchand, B. Goodman, and M. Chandrasekhar, *Phys. Rev. B* **71**, 174201 (2005).

<sup>18</sup>Q. Mei, P. V. Teredesai, C. J. Benmore, S. Sampath, E. Bychkov, J. Neufeind, K. Leinenweber, and J. L. Yarger, *Phys. Chem. Glasses* **46**, 483 (2005).

<sup>19</sup>M. V. N. Prasad, S. Asokan, G. Parthasarathy, S. S. K. Titus, and E. S. R. Gopal, *Phys. Chem. Glasses* **34**, 199 (1993).

<sup>20</sup>S. Asokan, M. V. N. Prasad, G. Parthasarathy, and E. S. R. Gopal, *Phys. Rev. Lett.* **62**, 808 (1989).

<sup>21</sup>M. Durandurdu and D. A. Drabold, *Phys. Rev. B* **65**, 104208 (2002).

<sup>22</sup>M. Shimada and F. Dache, *Inorg. Chem.* **16**, 2094 (1977).

<sup>23</sup>C. D. Martin, S. M. Antao, P. J. Chupas, P. L. Lee, S. D. Shastri, and J. B. Parise, *Appl. Phys. Lett.* **86**, 061910 (2005).

- <sup>24</sup>C. J. Benmore and P. S. Salmon, Phys. Rev. Lett. **73**, 264 (1994).
- <sup>25</sup>T. E. Faber and J. M. Ziman, Philos. Mag. **11**, 153 (1965).
- <sup>26</sup>D. A. Keen, J. Appl. Crystallogr. **34**, 172 (2001).
- <sup>27</sup>J. H. Hubbell, W. J. Veigle, E. A. Briggs, R. T. Brown, D. T. Cromer, and R. J. Howerton, J. Phys. Chem. Ref. Data **4**, 471 (1975).
- <sup>28</sup>V. F. Sears, Neutron News **3**, 26 (1992).
- <sup>29</sup>A. B. Bhatia and D. E. Thornton, Phys. Rev. B **2**, 3004 (1970).
- <sup>30</sup>P. S. Salmon, Proc. R. Soc. London, Ser. A **437**, 591 (1992).
- <sup>31</sup>P. S. Salmon and J. Liu, J. Phys.: Condens. Matter **6**, 1449 (1994).
- <sup>32</sup>I. Petri and P. S. Salmon, Phys. Chem. Glasses **43C**, 185 (2002).
- <sup>33</sup>Z. U. Borisova, *Glassy Semiconductors* (Plenum, New York, 1981).
- <sup>34</sup>U. Rütt, M. A. Beno, J. Stempfer, G. Jennings, C. Kurtz, and P. A. Montano, Nucl. Instrum. Methods Phys. Res. A **467-468**, 1026 (2001).
- <sup>35</sup>A. J. G. Ellison, R. K. Crawford, D. G. Montague, K. J. Volin, and D. L. Price, J. Neutron Res. **1**, 61 (1993).
- <sup>36</sup>J. D. Barnett, S. Block, and G. J. Piermarini, Rev. Sci. Instrum. **44**, 1 (1973).
- <sup>37</sup>K. H. Smith, E. Shero, A. Chizmeshya, and G. H. Wolf, J. Chem. Phys. **102**, 6851 (1995).
- <sup>38</sup>C. Meade and R. Jeanloz, in *High Pressure Research in Mineral Physics*, edited by M. H. Manghni and Y. Syono (American Geophysical Union, Washington, D.C., 1987), p. 41.
- <sup>39</sup>F. Birch, Phys. Rev. **71**, 809 (1947).
- <sup>40</sup>J. Urquidi, C. J. Benmore, J. Neuefeind, and B. Tomberli, J. Appl. Crystallogr. **36**, 368 (2003).
- <sup>41</sup>A. K. Soper, W. S. Howells, and A. C. Hannon, Report No. RAL-89-046, Rutherford Appleton Laboratory, Oxford, UK, 1989 (unpublished).
- <sup>42</sup>P. Verkerk, U. Bafle, F. Barocchi, L. A. de Graaf, J.-B. Suck, and H. Mutka, Phys. Rev. Lett. **67**, 1262 (1991).
- <sup>43</sup>R. A. Martin and P. S. Salmon (private communication).
- <sup>44</sup>A. P. Hammersley, Internal Report No. ESRF98HA01T, European Synchrotron Radiation Facility, Grenoble, France, 1998 (unpublished).
- <sup>45</sup>X. Qiu, J. W. Thompson, and S. J. L. Billinge, J. Appl. Crystallogr. **37**, 678 (2004).
- <sup>46</sup>A. C. Wright, J. Non-Cryst. Solids **179**, 84 (1994).
- <sup>47</sup>C. J. Benmore, R. T. Hart, Q. Mei, D. L. Price, J. Yarger, C. A. Tulk, and D. D. Klug, Phys. Rev. B **72**, 132201 (2005).
- <sup>48</sup>M. Durandurdu, Phys. Status Solidi B **242**, 3085 (2005).
- <sup>49</sup>G. Dittmar and H. Schäfer, Acta Crystallogr., Sect. B: Struct. Crystallogr. Cryst. Chem. **32**, 2726 (1976).
- <sup>50</sup>A. Grzechnik, T. Grande, and S. Stølen, J. Solid State Chem. **141**, 248 (1998).
- <sup>51</sup>Inorganic Crystal Structure Database, <http://icsd.ill.fr/icsd/>
- <sup>52</sup>A. Grzechnik, S. Stølen, E. Bakken, T. Grande, and M. Mezouar, J. Solid State Chem. **150**, 121 (2000).
- <sup>53</sup>M. Fuentes-Cabrera, H. Wang, and O. F. Sankey, J. Phys.: Condens. Matter **14**, 9589 (2002).
- <sup>54</sup>S. Stølen, A. Grzechnik, T. Grande, and M. Mezouar, Solid State Commun. **115**, 249 (2000).
- <sup>55</sup>L. W. Hobbs, C. E. Jesurum, V. Pulim, and B. Berger, Philos. Mag. A **78**, 679 (1998).
- <sup>56</sup>A. C. Wright, B. Bachra, T. M. Brunier, R. N. Sinclair, L. F. Gladden, and R. L. Portsmouth, J. Non-Cryst. Solids **150**, 69 (1992).